Strojniški vestnik - Journal of Mechanical Engineering 57(2011)4, 323-333
DOI:10.5545/sv-jme.2009.043

Paper received: 03.04.2009
Paper accepted: 11.01.2011

A Study of Quality Parameters and Behaviour of Self-Piercing Riveted Aluminium Sheets with Different Joining Conditions

Jacek Mucha*

*Rzeszow University of Technology, Faculty of Mechanical Engineering and Aeronautics, Poland

This paper presents research progress in the assembly dimensional prediction area, using finite element analysis results. A case study of the SPR of two sheets of the aluminium alloy using a steel rivet was investigated. The riveting analysis has been performed for joined sheets using finite element method (FEM) with MSC Marc Mentat software.

Thus, a simulated analysis was adopted in this study to improve industrial productivity. The comparison analysis has been performed within the numerical experiment range to cover the effect of various riveting process parameters on the rivet deformation. Proper selection of corresponding rivet material features, i.e. its yield point and strain hardening, enables significant changing of the sheet joining process and specific finished joint parameters. The finite element simulation is effective in determining the optimal conditions.

Keywords: joint formation, rivetion load, mechanical properties, finite element modelling

0 INTRODUCTION

Welding demands localized heating of the material, which may lead to changes in the mechanical properties of the materials. When searching for new solutions to replace the spot welding process, well-known press joining technology (for example: clinching, self-piercing riveting, cold pressure welding) capabilities have been recognized.

Cold pressure welding is a special welding method that has been used in applications such as assembly of various parts at an increasing rate in recent years. Cold pressure welding takes place due to the breakdown of the surface layers caused by bulk plastic deformation [1].

Self-piercing riveted (SPR) joints gain even larger share in the thin-walled structure assembly process in the metal industry, especially in the automotive industry so [2] and [3]. The latter one demands for the modern solutions for both the car design and the car production technology. As an example, the self-piercing riveting is used by Audi [4] and Jaguar [5] for joining car body pieces. Modern joining by forming technologies such as Self-Piercing Riveting are increasingly used in sheet metal processing industries owing to their many advantages. Moreover, these technologies are often interesting joining alternatives of new developed products with multi-material design and so on [6] to [9].

This is a submethod of pressed joints [10], and its basic benefit (in addition to the most important one – no bore drilling) is that various materials of different coating may joined, from painted and galvanized sheet metal, to plastic ones [11].

This method is used mostly for joining two or more thin sheets, which is acknowledged by the works of Han et al. [12]. The joint forming process is affected by several factors, which may be divided into relevant groups: geometrical factors, material factors, and technological factors [13].

The initial joined sheet hardening has a great meaning for the joining process and its quality indexes, which has been confirmed by Han et al. experimental research [14]. The work of Di Lorenzo and Landolfo [7] is also of great importance, where the analysis of joints made by various methods and strength tested was presented. When forming the joint, some joint execution correctness factors must be observed, as emphasized by Abe et al. [15] and Mori et al. [16]. Over the last few years, a rapid growth of the numerical computing methods based among the others on the finite element method (FEM) enabled analyzing a lot of issues related to such joint type

*Corr. Author's Address: Rzeszow University of Technology, Faculty of Mechanical Engineering and Aeronautics, W. Pola 2, 35-959 Rzeszów, Poland, j_mucha@prz.edu.pl

designing and performing. The application of modern research tools like professional computing FEM based software enables analyzing the virtual forming [17] to [22].

1 EXAMPLE JOINING OF ALUMINIUM SHEETS

During the SPR process, the self piercing rivet is pressed by a punch into two sheets, which are maintained between a blankholder and a lower tool.

The self-piercing riveting process can be described by the following four steps (Fig. 1):

- clamping (step I), the blank holder presses the two sheets against the die, and now the rivet is gradually pressed into aluminum sheets;
- piercing (step II), the punch pushes the rivet into the top plate;
- flaring (step III), the material of the lower sheet flows into the die and the rivet shank begins to flare outward, forming a mechanical interlock between the upper and lower substrates;
- release of the punch (IV step), finally, once the punch is retracted, the finished joint is achieved with the fastener properly seated in the sheets.

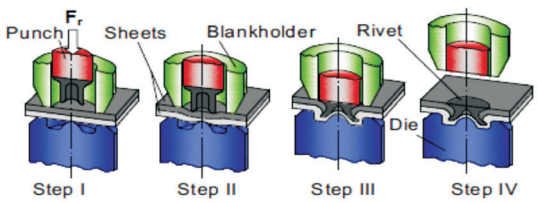

Fig. 1. *Schematic representation of the SPR process*

In particular, joint strength is determined by rivet flare into the locking sheet (reverse joint sheet), the dimensions of which are dependent on the profile. A typical internal die profile is shown in Fig. 2.

The use of the rivet, which indicates that the rivet has the characteristic shown in Fig. 3. The joint execution correctness may be assessed based on its appearance (Figs. 4b and c) and its cross section (Fig. 4d). The rivet is made of boron steel, and the sheets are aluminium alloy. The mechanical properties of the rivet (material model 1) and sheets are shown in Table 1. Sheet joining has been performed for selected sheet thickness arrangement (1.5/2 mm).

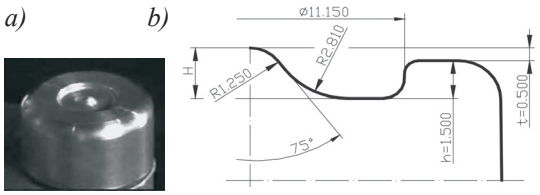

Fig. 2. *Used die as an alternative I; a) real appearance of a basic die by Böllhoff, b) its geometry*

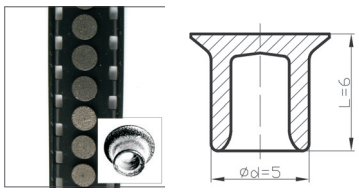

a) *b)*

Fig. 3. *Used rivet; a) real appearance, b) major dimensions*

Table 1. *Mechanical properties of the rivet and sheets*

Material		Young's Modulus E [GPa]	Yield stress $\sigma_{0.2}$ [MPa]	Material model	Flow stress [MPa]	
					C	n
Rivet	Boron steel	188	1520	1	2627	
			1176	2	1970	0.088
			980	3	1642	
			1520	4	1659	0.014
Sheets	Al. alloy	75	135	-	505	0.191

The flow stress of the rivet (material model 1) and sheets are obtained from the uniaxial compression and tensile tests, respectively, and the flow stress is used in the simulation. The material hardening effect has been described by the $\sigma = f(\varepsilon)$ relationship, using the equation:

$$\bar{\sigma} = C(\bar{\varepsilon})^n. \quad (1)$$

The C factor in this equation is called the strain hardening curve coefficient (material constant), and n is the strain hardening curve exponent.

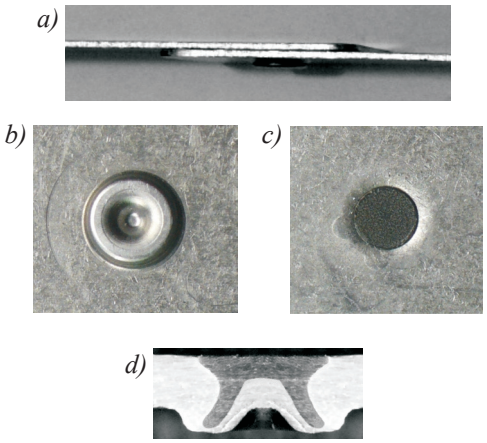

Fig. 4. *Example of final joint view; a) from the side, b) from the bottom, c) from the top, d) cross section*

Tests were carried out on two levels:

- material tests on the base material and on the rivet material were used to obtain the material properties used in the numerical models,
- riveting process tests using the new upsetting die.

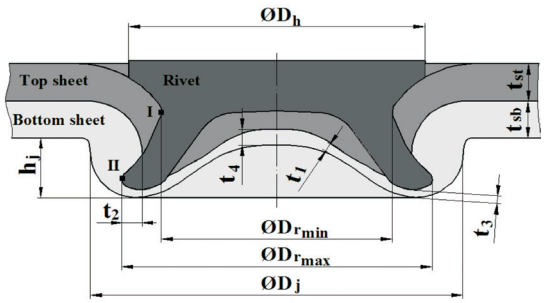

Fig. 5. *The characteristic parameters of SPR joint geometry*

2 JOINT ASSESSMENT PARAMETERS

SPR is designed for thin sheet joining and particular attention must be paid to essential indexes, which may affect the load carrying capacity for tangent and normal loads. The essential parameters for joint execution correctness assessment are presented on the cross section of a joint, see Fig. 5.

The final value of t_2 depends on the rivet spreading course, and also its interference in the lower sheet. The rivet response to specified boundary conditions of the process is e.g. its spreading course, which may be characterized by the course of its corresponding diameter ratio:

$$S_{Dr} = \frac{D_{r_{\max}}}{D_{r_{\min}}}. \tag{2}$$

Detailed recognition of the joining process enables optimal tooling selection based on e.g. riveting force value and the deformation of the pieces being joined.

3 THE NUMERICAL SIMULATION

Using the FEM simulation of the riveting process for specified parameters of the pieces being joined, the joining process and the join validity may be predicted. It will be possible to establish how and how much selected factors – geometrical, material and technological – affect the joining process. One of the objectives of the present paper is to simulate, utilizing the finite element method, the influence of changes in the riveting die and geometry on the material flow and consequent values parameter t_i SPR joints, which directly affect the joint strength.

3.1 Model of Simulation

The numerical computations have been performed in MSC Marc Mentat 2005 software, where an additional procedure enabling the material separation has been applied.

This procedure is based on the body mesh part separation effect in a location, where the part dimensions have gained the specified minimum value. When the upper sheet thickness reaches a user defined value the sheet is divided into two parts. This procedure allows the rivet to penetrate into the bottom sheet.

The upper sheet material thickness, where the mesh elements were split at their contact boundary, was set as 0.02 mm. At the end of each computation step the routine checks whether the distance between two nodes on the boundary of

selected material is not lower than the user defined distance. If the condition is met, two adjacent elements, for which the critical distance was observed, are split along the common edge.

A mesh size of 0.15 × 0.15 mm was used for the parts that were adaptively remeshed as well as for the remaining parts in order to reduce contact problems. Such defined parameters of mesh reconstruction enabled a stable solution of the issue in each computation step [21].

Due to a form of the joint itself and the course of forming, the self piercing riveting process may be considered using the two-dimensional axisymmetric model – the axisymmetric state of stress and strains [22]. The boundary conditions have been defined based on the SPR riveting (Fig. 1).

The sheets have been joined and the rivet has been modeled using the elastic-plastic material model with an isotropic hardening, using the quadrilateral axisymmetric element of type 10. As the problem is axisymmetric, the four node 2D axisymmetric elements have been used, with four Gauss points [23].

3.2 Conditions for Simulation

For purposes of detailed analysis of fastener strain course during the riveting, it has been decided to determine the characteristic points I and II (Fig. 5), nodes of the rivet mesh elements, which enable tracking the change of a diameter of a tubular part of the fastener, respectively for D_{rmin} and D_{rmax} (Fig. 5). Rivet spread ratio is measured for samples of each condition.

The rivet has enough hardness to piece the sheets, whereas the rivet is plastically deformed and the tubular leg of the rivet spreads. The joining process simulation has been performed for four rivet material models and one sheet material – see Table 1. It has been decided to perform the joining process simulation for other rivet material models (material model 2 to 4), Fig. 6.

The joined sheet and rivet yield point ratio significantly influences the joint creation process:

$$s_\sigma = \frac{\sigma_{02}^r}{\sigma_{02}^s}, \tag{3}$$

so this relationship has been additionally designated as S_σ. For the examined material models 1, 2, 3, 4, the S_σ value has been respectively: 11.26 (1), 8.71 (2), 7.26 (3) and 11.26 (4). Note that the difference of yield stresses for upper and lower sheet also affects the joint part behaviour when pressing the rivet. Note that the difference of yield stresses for upper and lower sheet also affects the joint part behaviour when pressing the rivet.

Due to a large number of variables in the form of input data, only one rivet geometry alternative has been used in the experiment. For all contact surfaces, the Coulomb friction model with the coefficient of friction μ = 0.05 has been adopted. In order to determine the coefficient friction effect on the joint forming process and riveting forces, the coefficient of friction μ = 0.1;

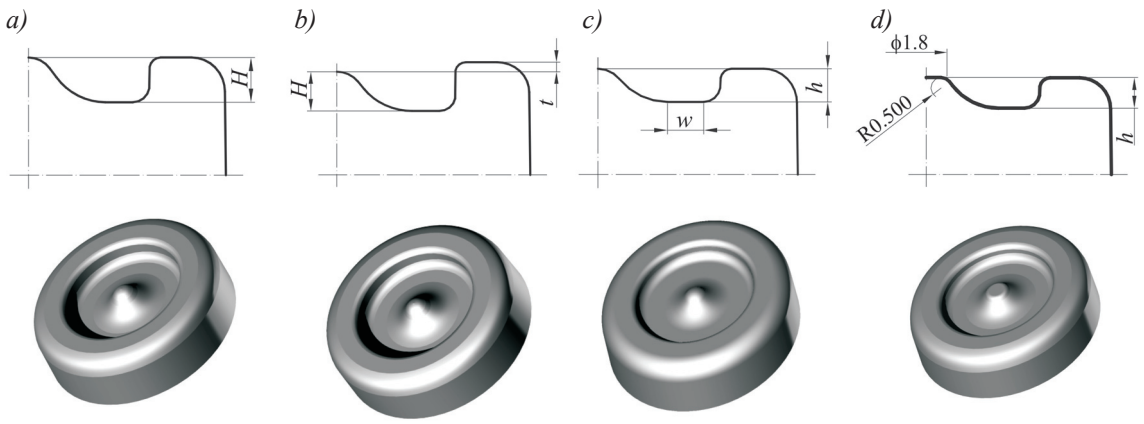

Fig. 7. *The general assumptions of die geometry with modified impression (var. II-V)*

0.15; 0.20; 0.25 has also been defined for the contact surface of the rivet and sheets.

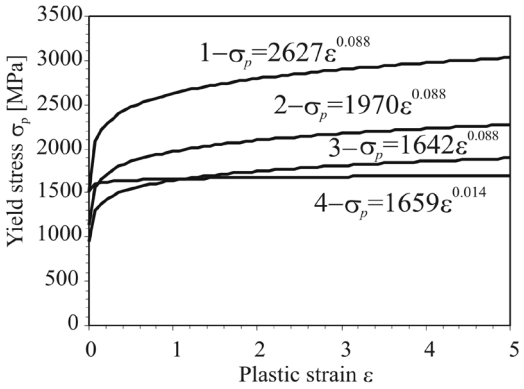

Fig. 6. *The strain hardening curves for various rivet models*

In order to analyze the effect of die impression form to the strain of joint pieces and riveting force levels, die models of various profiles (five) have been created and designated as follows:

- I, as a basic profile with the cone offset from the die bearing surface by 0.5 mm (see Fig. 2b),
- II, where the cone apex is located on the bearing surface level (same depth as in profile I), see Fig. 7a,
- III, with a bigger height of the bearing surface relative to the cone apex by 0.5 mm (see Fig. 7b),
- IV, for $h = H$ and eliminating the intermediate line between radius R 1.250 and R 2.810, and with increasing dimension w of the impression bottom by 0.37 (see Fig. 7c),
- V, where the truncated cone has been used (see Fig. 7d).

The numerical experiment has been limited to the sheets of identical material: *Al*/*Al*. In order to demonstrate the effect of the joined sheet thickness on the riveting process course and the joint quality indexes t_i, some determined arrangements have been used for the analysis. Based on a simple relationship, the upper to lower sheet thickness ratio index has been determined for the purposes of analysis:

$$\delta_t = \frac{t_{st}}{t_{sb}}, \tag{4}$$

and its values have been tabulated in Table 2. The remaining geometrical parameters, i.e. the die and rivet parameters have not been changed.

Table 2. *The joined sheet thickness ratio index*

Parameter	Value					
δ_t	0.5	0.6	0.7	0.8	0.9	1
t_{sb} [mm]	2					

4 RESULTS AND DISCUSSION

The author has decided to present the selected simulation results using 3D model, which has been achieved by expanding 2D axisymmetric joint model, achieved as a result of computations. The purpose was a better visualization of SPR joint form. Due to a large amount of information that may result from numerical computations, it has been decided to present the most important simulation results for:

- five alternatives of die impression,
- five different coefficient friction values between the rivet and sheets,
- six combinations of upper to lower sheet thickness ratio index,
- four models of rivet material for the same material model of joined sheets.

When analyzing the riveting force characteristics vs. punch displacement (Fig. 8) it can be said that the die impression *III* is the best solution due to the riveting force value. Let us look at the plastic strain distribution and joined element deformations (Fig. 9). For the die impression *III*, the finished joint has the highest number of imperfections, namely in areas 4, 5, and 6 (Fig. 9a) free spaces between individual joint elements may be observed, and those spaces may reduce the joint rigidity and load carrying capacity. The joint made with the die impression *II* has the lowest number of imperfections. The force required to make such a joint is higher by approx. 13500 N comparing to profile alternative *III*, however, it is also lower by approx. 15000 N than in profile alternative *I*.

Using the die with an alternative *IV* and *V* when joining, has no significant effect on the riveting, force curve and its maximum value. The profile *V* and *I* features the same maximum riveting force, but for the profile *IV* the maximum

riveting force was 48500 N. It has been decided not to place them on any chart for clarity purposes.

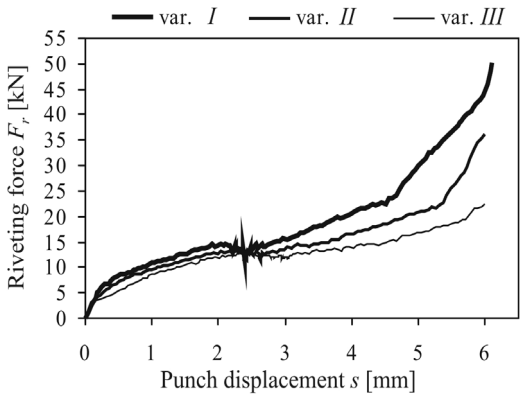

Fig. 8. *A comparison of riveting force curve for three profiles (rivet mat. 1, μ = 0.05, δ_t = 0.5)*

It is significant to note that by using the dies with various impressions it is possible to change the form and size of the joint itself. Fig. 10 presents the characteristics of the finished joint diameter change D_j vs. used die alternative.

For the die impression *III*, the lowest riveting force has been achieved (Fig. 8) at reduced D_j size (Fig. 10), however at the burden of joint height growth on the side of a flash. For all die impression form cases as referred to the above, the value of material shrinking (t_3) in an area 1 (Fig. 9a) was on a similar level. Its values and relations between the remaining indexes have been presented in Fig. 11. The local minimum for considered die alternatives may be observed on this chart. Due to a value of some indexes, the die impression profile *IV* seems to be the most

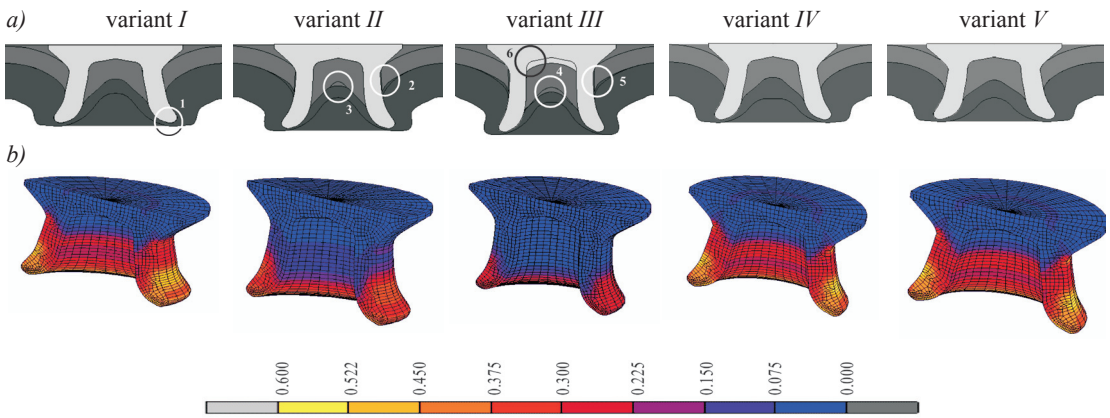

Fig. 9. *The view of the joint made with the die of five impression alternatives: a) joint cross section, b) plastic strain distribution in the rivet (rivet mat. 1, μ = 0.05, δ_t = 0.5)*

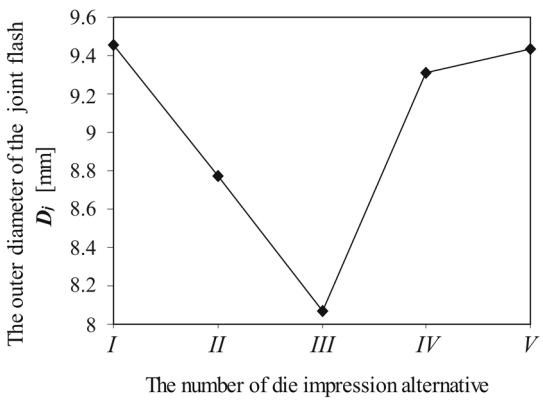

Fig. 10. *The outer diameter of the finished joint D_j (flash) vs. used die impression for joining (rivet mat. 1, μ = 0.05, δ_t = 0.5)*

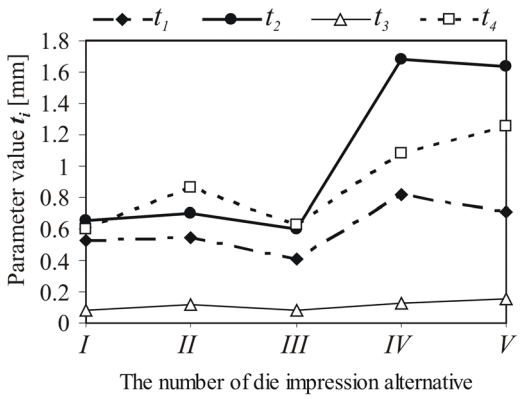

Fig. 11. *The t_i parameters for the joint made with die impression profile: I, II, III, IV, V (rivet mat. 1, μ = 0.05, δ_t = 0.5)*

effective for their highest values, as this has a significant meaning.

When riveting with the die impression profile *III* the lowest riveting force has been achieved (Fig. 8), but also the lowest caving t_2 of the rivet in the lower sheet (Fig. 11) and its spreading (Fig. 12). The value of caving significantly influences the finished joint strength properties.

In this way, the application of such a die impression is not a favourable solution in that case. In turn, for the die impression alternative *IV* the highest values of the rivet caving in the lower sheet t_2 and the second sheet shrank on the die cone t_1. The value of the rivet spread index for die impression alternative *II*, *IV*, *V* is basically on the same level (Fig. 12). From the high value t_i parameters preservation point of view, using the die impression form *IV* and *V* gives the best results for aluminum sheet joining.

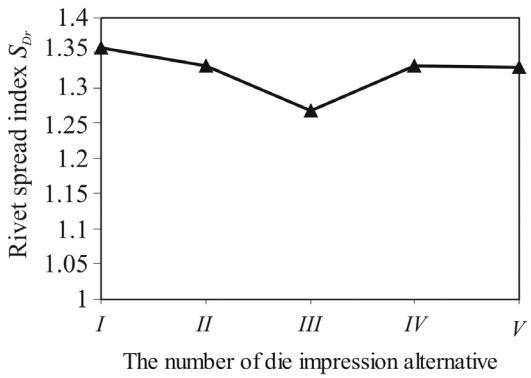

Fig. 12. *The effect of die impression form on the rivet spreading index in the finished joint (rivet mat. 1, μ = 0.05, δ_t = 0.5)*

The riveting force courses presented on Fig. 13 were determined based on the analysis of five models with different coefficients friction between the rivet and sheets. The friction between the rivet and the sheets has an influence on the results of the simulation, especially the friction between the rivet and the top sheet. The higher the value of the friction, the higher is the force needed to push the rivet though the sheet.

The final shape of the rivet shank and the part of the top sheet in contact with the tip of the rivet shank is influenced by friction. Such a defined coefficient friction in the model does not significantly affect the maximum riveting force and the die impression filling. This is a factor, which significantly affects the value and the range of plastic strains in joined sheets and joint element deformation, see Fig. 14. The higher value the coefficient of friction, the higher are joint element deformations and material separation delay. This may be explained by the fact that at higher coefficient friction values, the material displacement resistance on the body contact boundary increases.

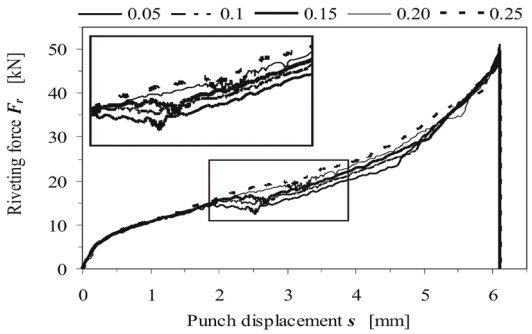

Fig. 13. *The riveting force course vs. punch displacement for different coefficients friction between the rivet and joined sheets (die var. I, rivet mat. 4, δ_t = 0.5)*

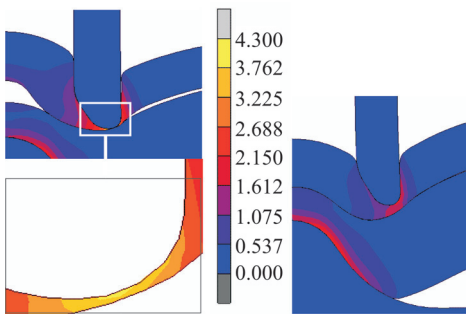

a) *b)*

Fig. 14. *The comparison of the equivalent plastic strain distribution and joint element deformation at the same punch path for the model with μ between rivet and sheets; a) 0.05, b) 0.25 (die var. I, rivet mat. 4, δ_t = 0.5)*

For different combinations of sheet thickness ratio t_{st}/t_{sb}, the fastener (with specified material properties) sooner or later expands in

the created joint. The simulation results in form of individual index values and their courses for corresponding joint alternatives was placed in the charts, see Figs. 15 and 16. The higher the upper to lower sheet thickness ratio dt, the higher are the values of parameter t_3, both for the rivet material model 1 and 3. The remaining parameters, i.e. t_1, t_2, t_4 decrease while the upper sheet increases for each presented rivet material model.

Specific rivet material properties, e.g. the yield point and the hardening curve course, significantly affect the value of t_i parameters during the joining process.

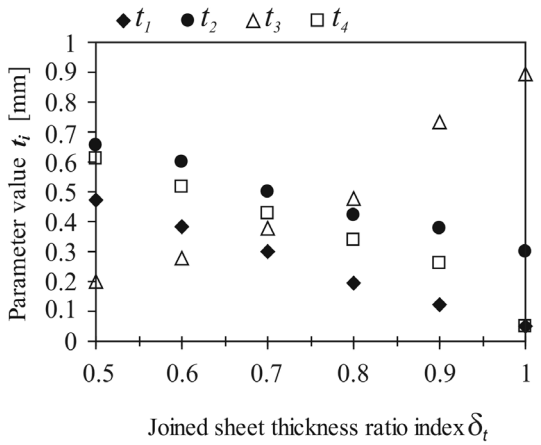

Fig. 15. *The effect of joined sheet thickness ratio index δ_t during the riveting on final parameters t_i (die var., I, rivet mat., 3, μ = 0.05)*

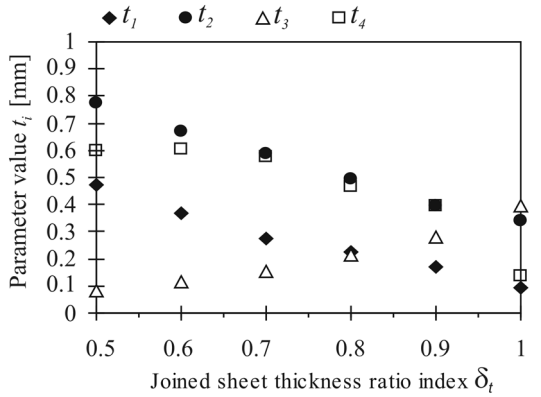

Fig. 16. *The effect of joined sheet thickness ratio index $\boldsymbol{\delta_t}$ during the riveting on final parameters $\boldsymbol{t_i}$ (die var. I, rivet mat. 1, μ = 0.05)*

The relations between specific parameters ti and their course are presented in Fig. 17, where some regularity may be observed. The parameter t_2 increases and t_3 decreases while the resistance of the rivet material to plastic strain increases. This is due the increased rivet rigidity, which is responsible for specific sheet material flow in the die impression.

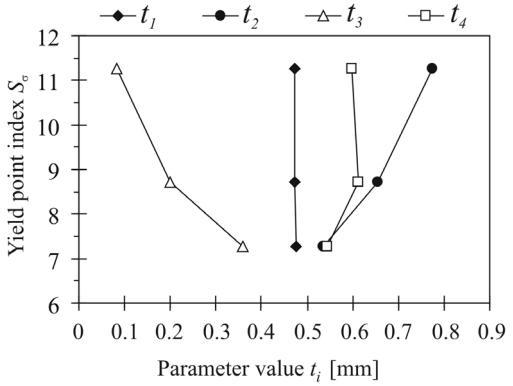

Fig. 17. *The effect of sheet and rivet yield point index to $\boldsymbol{t_i}$ parameter variations for joined aluminum sheet (rivet mat. 1-3, die var. – I, μ = 0.05)*

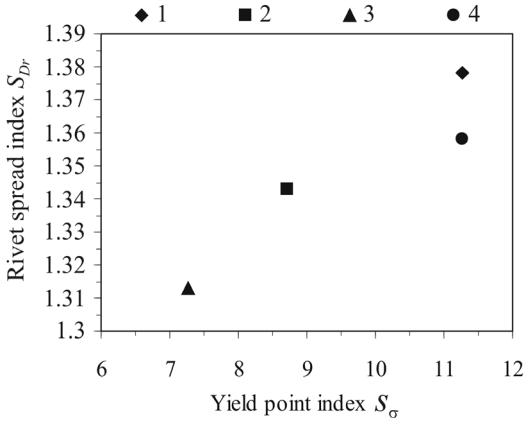

Fig. 18. *The effect of sheet and rivet yield point index to the rivet expansion index in the finished joint (rivet mat. 1 to 4, die var., I, μ = 0.05, δ_t = 0.5)*

The rivet material response during its pressing is its hardening due to corresponding plastic strains. With a diversified rivet material hardening characteristics different behavior of rivet material may be found during the joining process (Fig. 18). The higher yield point ratio index S_σ,

the higher rivet spread index values are achieved in the joint. The selection of corresponding rivet material features, i.e. plastifying strain and its hardening curve course significantly affects the joint forming process and the final result in form of parameters t_i, S_{Dr}, which finally is reflected in the load carrying capacity. In addition to the yield point the material hardening curve course should also be accounted for when selecting the rivet material for the specified combination of joined sheet mechanical properties.The difference of yield stresses for upper and lower sheet also affects the joint part behaviour when pressing the rivet. However, this requires a separate analysis.

5 CONCLUSIONS

The numerical FEM simulation results may be used when designing those modern joints both for other arrangements of joined sheet mechanical properties and the technology used to create them. Once the analysis has been performed, detailed conclusions were achieved and the most important conclusions are presented as follows:

- One of the significant factors affecting the finished joint form is the die impression geometry. Proper selection of die impression enables riveting force reduction and achievement of the smallest flash diameter of the finished joint. Lowering the conical part of die impression (i.e. making it flush with a die face) and decreasing the impression depth resulted in the highest value of most t_i indicators;
- Proper selection of corresponding rivet material features, i.e. its yield point and strain hardening, enables a significant change of the sheet joining process and specific finished joint parameters;
- The energy consumption for the rivet strain depends, among else, on the strain hardening curve. The final joint parameters (t_i) and the energy needed to the rivet material strain should be considered when selecting the rivet material (see Fig. 6).

The total forming energy dissipation rate in this case is obtained by summing-up all the energy dissipation rates, which are caused by the internal plastic deformation, shear at the velocity discontinuities and due to friction at the tool-material interfaces, i.e.

$$\dot{E}_T = \dot{E}_i + \dot{E}_s + \dot{E}_f, \tag{5}$$

where:

$\dot{E}_i$ is the internal energy dissipation rates due to plastic deformation,
$\dot{E}_s$ is the energy dissipation rates along the velocity discontinuity surfaces,
$\dot{E}_f$ is the frictional energy dissipation rates.

The internal energy dissipation rates due to plastic deformation are defined as:

$$\dot{E}_i = \int_V \sigma_{ij}\dot{\varepsilon}_{ij} dV, \tag{6}$$

where:

σ_{ij} stress tensor,
$\dot{\varepsilon}_{ij}$ strain-rate tensor,
V the volume.

Shear energy dissipation rates can be obtained using the following equation:

$$\dot{E}_s = k\int_A |\Delta v| dA, \tag{7}$$

where k, $|\Delta v|$ and A are the yield shear stress, the change of velocity at the velocity discontinuity surface and the area of the surface, respectively. The value of $k = \bar{\sigma}/\sqrt{3}$.

The frictional energy dissipation rates at the tool material interfaces may be determined using the basic equation:

$$\dot{E}_f = \int_A \tau |\Delta v| dA = mk\int_A |\Delta v| dA, \tag{8}$$

where τ and m are the shear stress at the frictional surface and the friction shear factor which is assumed to be a constant over the surface, irrespective of the pressure between them and the velocity between the tool and the material, and this may be taken as $\tau = m \cdot k$, with $0 \le m \le 1$.

The external energy rate of deformation is forming load:

$$F_r V_p = \dot{E}_t, \tag{9}$$

where:

F_r the riveting force,
V_p velocity punch.

Hence,

$$F_r = \frac{\dot{E}_t}{V_p}. \quad (10)$$

The enclave of the plastic region, the deformed geometry, the punch load, and the value of parameters t_i can be predicted by the finite element model. This information can be used to improve the manufacturing process and the design of tools. In the future, more precise optimization of the components will be possible by transferring data from previous stages of sheet forming and joining to the structural computation code.

6 REFERENCES

[1] Ozel, K., Sahin, M., Akdogan, A. (2008). Mechanical and metallurgical properties of aluminium and copper sheets joined by cold pressure welding. *Strojniški vestnik - Journal of Mechanical Engineering*, vol. 54, no. 11, p. 796-806.

[2] Barnes, T.A., Pashby, I.R. (2000). Joining techniques for aluminium spaceframes used in automobiles, Part 2 – Adhesive bonding and mechanical fasteners. *Journal of Materials Processing Technology*, vol. 99, no. 1-3, p. 72-79.

[3] Mucha, J. (2007). Modern mechanical on press joinability techniques for sheet metal elements. *Proceedings of the International Scientific Conference Progressive Technologies and Materials in Engineering*, Pro-Tech-Ma`07, p. 43-44.

[4] Kochan, A. (2000). Audi moves forward with all aluminium cars. *Assembly Automation*, vol. 20, no. 2, p. 132-135.

[5] Mortimer, J. (2001). Jaguar uses X350 car to pioneer use of self-piercing rivets. *Industrial Robot: An International Journal*, vol. 28, no. 3, p. 192-198.

[6] Carle, D., Blount, G. (1999). The suitability of aluminium as an alternative material for car bodies. *Materials and Design*, vol. 20, no. 5, p. 267-272.

[7] Di Lorenzo, G., Landolfo, R. (2004). Shear experimental response of new connecting systems for cold-formed structures, *Journal of Constructional Steel Research*, vol. 60, no. 3-5, p. 561-579.

[8] Varis, J. (2006). Economics of clinched joint compared to riveted joint and example of applying calculations to a volume product. *Journal of Materials Processing Technology*, vol. 172, no. 1, p. 130-138.

[9] Mucha, J. (2007). History of the riveted joint technique (Self Piercing Riveting – SPR). *Mechanik*, vol. 80, no. 5-6, p. 454-460.

[10] Mucha, J. (2007). Classification and characteristic of the riveted joints without making holes. *Technologia i Automatyzacja Montażu*, vol. 58, no. 4, p. 7-10.

[11] Pickin, C.G., Young, K., (2007). Tuersley I. Joining of lightweight sandwich sheets to aluminium using self-pierce riveting. *Materials and Design*, vol. 28, no. 8, p. 2361-2365.

[12] Han, L., Chrysanthou, A., Young, K.W. (2007). Mechanical behaviour of self-piercing riveted multilayer joints under different specimen configurations. *Materials and Design*, vol. 28, no. 7, p. 2024-2033.

[13] Mucha, J. (2008). The influence of shape of tool die and blankholder on effect of deformation joint elements and rivetion load values. *Acta Mechanica Slovaca*, vol. 12, no. 3, p. 279-286.

[14] Han, L., Young, K.W., Chrysanthou, A., O'Sullivan, J.M. (2006). The effect of pre-straining on the mechanical behaviour of self-piercing riveted aluminium alloy sheets. *Materials and Design*, vol. 27, no. 10, p. 1108-1113.

[15] Abe, Y., Kato, T., Mori, K. (2006). Joinability of aluminium alloy and mild steel sheets by self piercing rivet. *Journal of Materials Processing Technology*, vol. 177, no. 1-3, p. 417-421.

[16] Mori, K., Kato, T., Abe, Y., Ravshanbek, Y. (2006). Plastic joining of ultra high strength steel and aluminium alloy sheets by self piercing rivet. *CIRP Annals – Manufacturing Technology*, vol. 55, no. 1, p. 283-286.

[17] Porcaro, R., Hanssen, A.G., Langseth, M., Aalberg, A. (2006). Self-piercing riveting process: An experimental and numerical investigation. *Journal of Materials Processing Technology*, vol. 171, no. 1, p. 10-20.

[18] De Paula, A.A., Aguilar, M.T.P., Pertence, A.E.M., Cetlin, P.R. (2007). Finite element simulations of the clinch joining of metallic sheets. *Journal of Materials Processing Technology*, vol. 182, no. 1-3, p. 352-357.

[19] Mucha, J. (2009). Numeric study of the phenomena occurring in the self piercing riveting process, *Mechanik*, vol. 82, no. 4, p. 286-291.

[20] Mucha, J. (2009). Some aspects of designing process self piercing riveting. *Archives of Mechanical Technology and Automation*, vol. 29, no. 4, p. 91-101.

[21] Bouchard, P.O., Laurent, T., Tollier, L. (2008). Numerical modeling of self-pierce riveting – From riveting process modeling down to structural analysis. *Journal of Materials Processing Technology*, vol. 202, no. 1-3, p. 290-300.

[22] Atzeni, E., Ippolito, R., Settineri, L. (2009). Experimental and numerical appraisal of self-piercing riveting. *CIRP Annals – Manufacturing Technology*, vol. 58, no. 1, p. 17-20.

[23] MSC (2005). *SuperForm*, *User`s Guide*.

[24] MSC (2005). *Marc, Theory and user information*, Volume A.

[25] MSC (2005). *Marc, Element library*, Volume B.